PNAS RESEARCH ARTICLE | NEUROSCIENCE OPEN ACCESS

ARL6IP1 mediates small-molecule-induced alleviation of Alzheimer pathology through FXR1-dependent BACE1 translation initiation

Gui-Feng Zhou[a], Jing Tang[a], Yuan-Lin Ma[a], Xian Fu[b], Jun-Yan Liu[b], Ren-Zhi Yang[c], Hong-Sheng Zhang[c], Xiang-Hai Cai[d], Jing-Wen Wang[a], Xiao-Yong Xie[a], Li Song[a], Biao Luo[a], Jian Chen[a], Long Chen[a], Xiao-Juan Deng[a], and Guo-Jun Chen[a,1]

Edited by Gregory Petsko, Brigham and Women's Hospital Center for Neurologic Diseases, Boston, MA; received December 7, 2022; accepted April 17, 2023

Exploring the potential lead compounds for Alzheimer's disease (AD) remains one of the challenging tasks. Here, we report that the plant extract conophylline (CNP) impeded amyloidogenesis by preferentially inhibiting BACE1 translation via the 5′ untranslated region (5′UTR) and rescued cognitive decline in an animal model of APP/PS1 mice. ADP-ribosylation factor–like protein 6–interacting protein 1 (ARL6IP1) was then found to mediate the effect of CNP on BACE1 translation, amyloidogenesis, glial activation, and cognitive function. Through analysis of the 5′UTR-targetd RNA-binding proteins by RNA pulldown combined with LC-MS/MS, we found that FMR1 autosomal homolog 1 (FXR1) interacted with ARL6IP1 and mediated CNP-induced reduction of BACE1 by regulating the 5′UTR activity. Without altering the protein levels of ARL6IP1 and FXR1, CNP treatment promoted ARL6IP1 interaction with FXR1 and inhibited FXR1 binding to the 5′UTR both in vitro and in vivo. Collectively, CNP exhibited a therapeutic potential for AD via ARL6IP1. Through pharmacological manipulation, we uncovered a dynamic interaction between FXR1 and the 5′UTR in translational control of BACE1, adding to the understanding of the pathophysiology of AD.

conophylline | ARL6IP1 | 5′UTR | FXR1 | BACE1 translation

Significance

In Alzheimer's disease (AD), BACE1 links the key molecular alterations with toxic Aβ overload, and pharmacological regulation of BACE1 may facilitate the discovery of novel mechanisms. We report such a small-molecule conophylline (CNP) that inhibits BACE1 translation through the 5′ untranslated region (5′UTR). Mediated by its target ARL6IP1, the brain-penetrating CNP attenuates amyloidogenesis and rescues cognitive decline in APP/PS1 mice. Upon CNP treatment, an enhanced interaction of ARL6IP1 with FXR1, which is identified as the 5′UTR-targeted protein, allows to sequester FXR1 from the 5′UTR, leading to the reduced translation of BACE1. Collectively, whereas CNP exhibits a therapeutic potential for AD through ARL6IP1, a dynamic FXR1–RNA interaction in the translational control of BACE1 is highlighted.

In the current Alzheimer's disease (AD) drug pipeline, the disease-modifying therapies (DMTs) account for more than 80% of the candidate treatment (1, 2). The drug targets are largely based on mechanisms, which include inflammation and synaptic plasticity. Despite the complicated factors associated with the disease risk (3), Aβ and Tau explicitly contribute to the formation of the pathological hallmarks of AD and are crucial for diagnosing disease and judging treatment effect (4). Thus, the pathology-based DMT provides an alternative strategy for drug searching, which, conversely, would allow to explore the potential upstream events beyond those identified by multiomics approach (5–7).

β-site amyloid precursor protein cleaving enzyme 1 (BACE1) is considered as the β-secretase that initiates the generation of Aβ (8, 9). While potent BACE1 inhibitors significantly decrease amyloid deposition in the brain, they fail clinical trials (10, 11), which could be partially associated with the decreased synaptic vesicle release (12). On the contrary, BACE1 "crosstalks" with a variety of cellular dysfunctions (13). Oxidative stress, inflammation, and calcium disturbances that contribute to BACE1 activation are also closely associated with the progression of AD (14). In this respect, a drug development could employ BACE1 expression as a "readout" for bridging Aβ generation to the potential regulatory mechanisms. Meanwhile, reducing protein in amount would allow the remaining BACE1 to be functional, thus avoiding the off-target effects by the structure-based protein inhibitors.

ADP-ribosylation factor–like GTPase 6–interacting protein 1 (ARL6IP1) is a tetraspan membrane protein that helps shape endoplasmic reticulum (ER) tubules in mammalian cells (15). Deletion of ARL6IP1 causes an increase of ER sheets and disrupts mitochondrial network organization (16, 17). It is reported that a single frameshift variant causes spastic paraplegia (18), and the truncating variant also leads to developmental delay, microcephaly, and neonatal hypotonia (19, 20). In line with this, knockdown of ARL6IP1 results in microphthalmia and defects in neural crest migration in zebrafish (21, 22). Yet, whether ARL6IP1 might be involved in AD is currently unclear.

Using live-cell high-throughput small-molecule screening, we have previously reported that the matrix metallopeptidase 13 (MMP13) inhibitor CL82198 controls BACE1 translation that is dependent on the 5′ untranslated region (5′UTR) (23), and a flavonoid cosmosiin regulates amyloidogenesis by promoting the 5′UTR-dependent translation of a disintegrin and metalloproteinase domain–containing protein

Author contributions: G.-J.C. designed research; G.-F.Z., J.T., Y.-L.M., X.F., J.-Y.L., R.-Z.Y., H.-S.Z., X.-H.C., J.-W.W., X.-Y.X., L.S., B.L., J.C., and L.C. performed research; X.-J.D. contributed new reagents/analytic tools; G.-F.Z. analyzed data; J.T., X.F., J.-Y.L., R.-Z.Y., H.-S.Z., X.-H.C., J.-W.W., X.-Y.X., L.S., B.L., J.C., L.C., and X.-J.D. provided assistance with the research; and G.-F.Z. and G.-J.C. wrote the paper.

Competing interest statement: Conophylline has been patented by China National Intellectual Property Administration.

This article is a PNAS Direct Submission.

[1]To whom correspondence may be addressed. Email: woodchen2015@163.com.

This article contains supporting information online at https://www.pnas.org/lookup/suppl/doi:10.1073/pnas.2220148120/-/DCSupplemental.

Published May 22, 2023.

(ADAM10) (24). This approach leads to the finding of the plant extract conophylline (CNP) in the current study. We define that CNP inhibits BACE1 translation via the 5′UTR and recues cognitive decline of APP/PS1 mice, which is mediated by ARL6IP1, the target molecule of CNP. The potential mechanism involves the enhanced interaction between ARL6IP1 and FMR1 autosomal homolog 1 (FXR1), and in parallel, the reduced FXR1–5′UTR binding and BACE1 translation. Our results highlight that CNP exhibits a therapeutic potential for AD, in which ARL6IP1–FXR1–5′UTR interactions in BACE1 translation are dynamically regulated.

Results

CNP Inhibited BACE1 Translation via the 5′UTR in Human SH-SY5Y Cells. CNP is known to inhibit pancreatic fibrosis and liver cirrhosis, and activate autophagy (25). The anticancer activity is also recently found (26). To determine whether CNP might be involved in amyloidogenesis, we first assessed the protein levels of APP, the two catalytic enzymes ADAM10 and BACE1, and the related APP products α/β-CTF, sAPPα/β, and Aβ species, in SH-SY5Y cells treated with CNP. As shown in Fig. 1*A*, CNP significantly decreased the protein level of BACE1 (*SI Appendix*, Fig. S1) without altering that of APP and ADAM10, which was paralleled with the reduction of sAPPβ and β-CTF (Fig. 1*B*). Whereas the protein level of sAPPα was not altered by CNP, that of α-CTF was reduced (Fig. 1*B*), along with the reduction of Aβ levels (Fig. 1*C*). Dose–response effect showed that the effective concentrations ranged from 100 to 250 ng/ml without obvious toxicity (Fig. 1 *D* and *E*), and the time-course response revealed that the BACE1-reducing effect of CNP (100 ng/mL) lasted for up to 48 h (Fig. 1*F*). Immunofluorescent images further confirmed that BACE1 protein in SH-SY5Y cell (*SI Appendix*, Fig. S1) was significantly reduced by CNP (Fig. 1*G*). Interestingly, CNP did not alter BACE1 at mRNA levels (Fig. 1*H*), suggesting a posttranscriptional mechanism. Thus, we assessed the involvement of protein degradation pathway with the lysosomal and proteosomal inhibitors chloroquine (CQ) and MG132, respectively. As shown in Fig. 1*I*, although the basal protein level of BACE1 was significantly increased by CQ or MG132, these agents failed to prevent CNP-induced reduction of BACE1. We further found that in the presence of translation inhibitor cycloheximide (CHX) but not transcription inhibitor actinomycin D (ActD), CNP-induced reduction of BACE1 protein level was significantly attenuated (Fig. 1*J*). Finally, in cells transfected with a plasmid in which the 5′UTR of BACE1 or ADAM10 was cloned into a luciferase reporter, the luciferase activity of BACE1-5′UTR but not ADAM10-5′UTR was significantly reduced by CNP (Fig. 1*K*), indicating that CNP preferentially inhibited BACE1 translation via the 5′UTR.

CNP Rescued Cognitive Decline in APP/PS1 Mice by Inhibiting BACE1. We next examined the effect of CNP in murine (HT22) cells. As shown in Fig. 2 *A*–*C*, CNP significantly reduced BACE1 protein levels at concentrations of 100 to 250 ng/mL without overt cytotoxicity, and the BACE1-reducing effect of CNP (100 ng/mL) lasted for up to 48 h in HT22 cells. In addition to neurons, CNP also reduced BACE1 expression in microglia and astrocytes in vitro and in the hippocampus of APP/PS1 mice (*SI Appendix*, Fig. S2), suggesting that CNP was functional in multiple cell types in the brain. Indeed, CNP showed a strong capability to penetrate blood–brain barrier (BBB), as the concentration of CNP was detected in the blood and brain homogenate starting at 30 min after i.p. injection, and remained high and stable for up to 72 h (Fig. 2*D*), the very long half-life of CNP was reminiscent to other psychotropic drugs (27). In WT mice, CNP administration significantly decreased the protein level of BACE1 without altering α/β-CTF (Fig. 2*E*), consistent with previous report that partial reduction of BACE1 does not alter CTF levels in normal mice (28). In APP/PS1 mice, however, CNP treatment led to a significant reduction of BACE1 and α/β-CTF (Fig. 2*E*). It is reported that BACE1 inhibitor LY2811376 causes significant changes in Aβ and sAPPα in human subjects (29), and seizure-related 6 homolog (SEZ6) is one of the best characterized substrates of BACE1 (30, 31). To further determine whether CNP-induced alteration of sAPPα and α/β-CTF was associated with BACE1, we compared the effect of CNP with LY2811376 in 5×FAD mice, another mouse model of AD, by assessing the protein levels of full-length (FL-SEZ6) and soluble SEZ6 (sSEZ6) in addition to sAPPα/β and α/β-CTF. As shown in Fig. 2*F*, in both CNP- and LY2811376-treated mice, the protein level of FL-SEZ6, as opposed to that of sSEZ6, was significantly increased, and the significant elevation of sAPPα was with the concomitant reduction of sAPPβ and α/β-CTF levels. Moreover, LY2811376 also reduced α/β-CTF in human SH-SY5Y cells with γ-secretase inhibitor DAPT (*SI Appendix*, Fig. S3), thus mimicking the effect of CNP (Fig. 1*B*). We further found that Aβ40/42 levels in the hippocampus of APP/PS1 mice were accordingly reduced by CNP (Fig. 2*G*). Moreover, as shown in Fig. 2 *H*–*K*, the escape latency, the passing times, and the staying time in the target quadrant were significantly altered by CNP in APP/PS1 mice, indicating that CNP improved the cognitive functions in APP/PS1 mice.

ARL6IP1 Mediated CNP-Induced Attenuation of AD-Like Pathology and Cognitive Deficits. It is reported that ARL6IP1 is a target protein of CNP (32). To determine whether ARL6IP1 is involved in CNP function, we then assessed the effect of ARL6IP1 knockdown (KD) (*SI Appendix*, Fig. S4) on BACE1 expression and amyloidogenesis in cultured cells. As shown in Fig. 3 *A* and *B*, ARL6IP1 KD significantly reduced the protein levels of BACE1 and Aβ40/42 in SH-SY5Y cells. Moreover, ARL6IP1 KD significantly reduced the basal 5′UTR-lucierase activity and further diminished CNP-induced reduction, indicating that the 5′UTR-dependent regulation of BACE1 by CNP was mediated by ARL6IP1 (Fig. 3*C*). Indeed, in cells transiently transfected with ARL6IP1 siRNA, CNP failed to further reduce BACE1 protein levels (Fig. 3*D*). To further verify that CNP-induced alleviation of AD-like pathology is mediated by ARL6IP1 in vitro, we assessed the protein levels of BACE1 and amyloidogenesis in APP/PS1 mice, using AAV-mediated delivery of shARL6IP1 in the hippocampus (*SI Appendix*, Fig. S4). As shown in Fig. 3*E*, ARL6IP1 silencing (shARL) significantly reduced the protein levels of BACE1, sAPPβ, and β-CTF (lane 3 vs. lane 1). Whereas the protein levels of BACE1, sAPPβ, and β-CTF were significantly reduced by CNP in APP/PS1 mice in control (shNC), they were not significantly changed by CNP in shARL (lane 3 vs. lane 4). Consistently, Aβ40/42 levels and Aβ plaque loads were significantly reduced by shARL or CNP alone, but no significant changes were found between shARL and CNP (Fig. 3 *F* and *G*, and *SI Appendix*, Fig. S4*D*). To determine whether shARL might influence neurodegeneration, we assessed degenerating cells and apoptosis using Fluoro-Jade C (FJC) staining and terminal deoxynucleotidyl transferase dUTP nick end labeling (TUNEL), respectively (33, 34). As shown in Fig. 3 *H* and *I*, ARL6IP1 knockdown significantly decreased FJC-positive cells and apoptosis rate measured by percent TUNEL-positive over DAPI-positive cells and further prevented the effect of CNP in APP/PS1 mice. Because

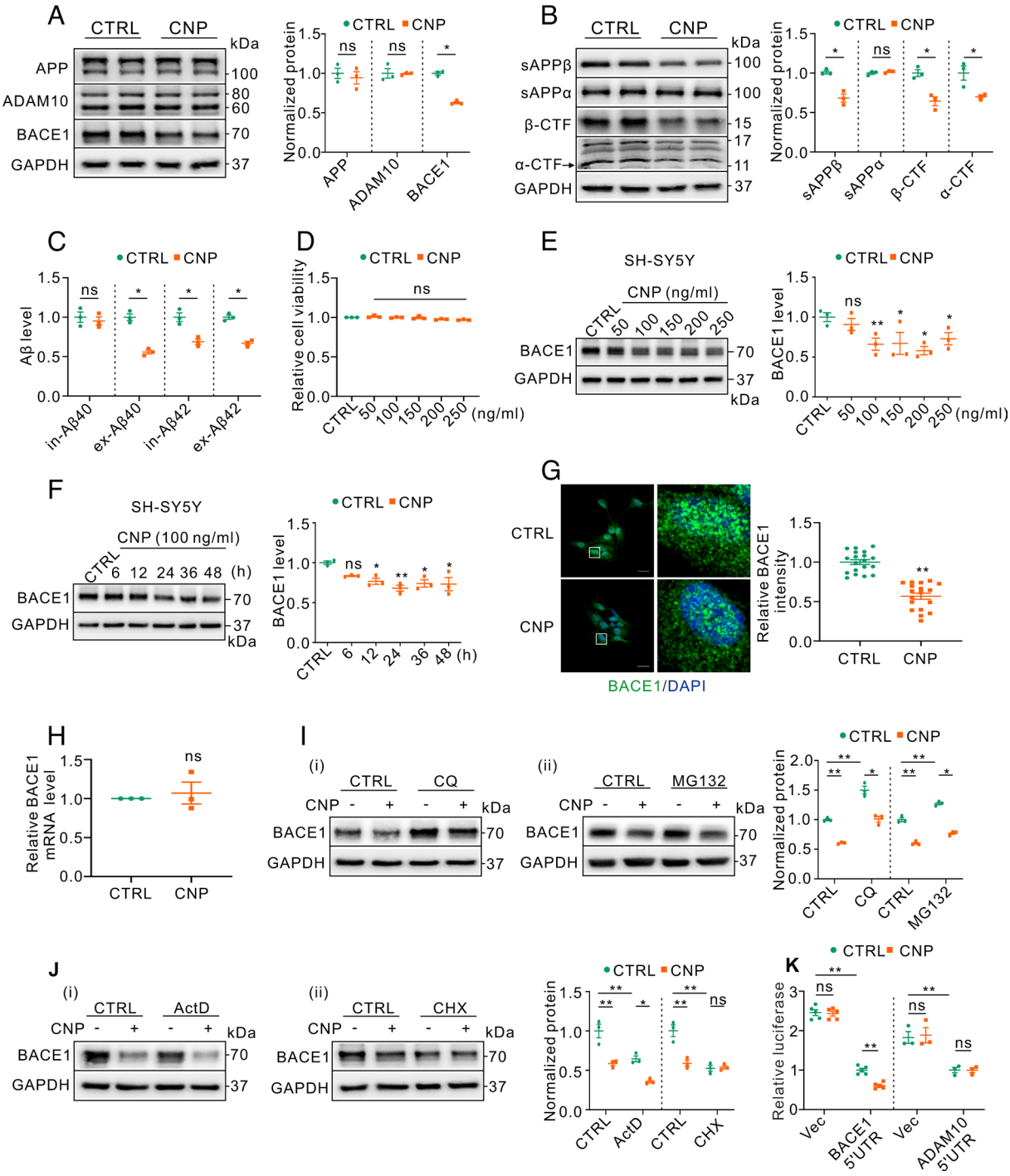

Fig. 1. CNP reduces BACE1 translation via the 5′UTR. (*A*) Representative western blots (*Left*) and quantification (*Right*) of APP, ADAM10, and BACE1 in SH-SY5Y cells were treated without (CTRL) or with CNP (100 ng/mL) for 24 h. Antibody information: APP (Sigma, A8717), ADAM10 (Abcam, ab124695), BACE1 (Abcam, ab108394). (*B*) Representative western blots (*Left*) and quantification (*Right*) of sAPPα/β and α/β-CTF in SH-SY5Y cells were treated without (CTRL) or with CNP (100 ng/mL) for 24 h. For better detection of α/β-CTF, γ-secretase inhibitor DAPT (250 nM) was incubated with CNP. Antibody information: sAPPβ (BioLegend, SIG-39138), sAPPα and β-CTF (IBL, 2B3), α-CTF (Sigma, A8717). (*C*) Aβ40 and Aβ42 levels in cell lysates (intracellular, in) and culture medium (extracellular, ex) were measured by ELISA, and SH-SY5Y cells were treated without (CTRL) or with CNP (100 ng/mL) for 24 h. (*D*) Relative cell viability of SH-SY5Y cells treated with CNP (0 to 250 ng/mL) for 24 h. (*E* and *F*) Dose–response effect (*E*) and time-course effect (*F*) of CNP on BACE1 protein levels in SH-SY5Y cells. BACE1 antibody: Abcam, ab108394. (*G*) Representative immunostaining (*Left*) and quantification (*Right*) of BACE1 in SH-SY5Y cells were treated without (CTRL) or with CNP (100 ng/mL) for 24 h. BACE1(green), DAPI (blue). (Scale bar: 25 μm.) BACE1 antibody: Abcam, ab183612. (*H*) Relative BACE1 mRNA levels in SH-SY5Y cells were treated without (CTRL) or with CNP (100 ng/mL) for 24 h. (*I*) BACE1 protein levels in SH-SY5Y cells treated with CNP (100 ng/mL) for 24 h in the absence or presence of lysosome inhibitor chloroquine (CQ, 100 μM for 6 h) (*i*) or proteasome inhibitor MG132 (1 μM for 6 h) (*ii*). BACE1 antibody: Abcam, ab108394. (*J*) BACE1 protein levels in SH-SY5Y cells were treated with CNP (100 ng/mL) for 24 h in the absence or presence of inhibitor actinomycin D (ActD, 0.1 μM for 12 h) (*i*) or translation inhibitor cycloheximide (CHX, 10 μM for 6 h) (*ii*). BACE1 antibody: Abcam, ab108394. (*K*) Relative luciferase activities in SH-SY5Y cells transiently transfected with the luciferase reporter plasmid pmirGLO/pGL4.51 that was without (Vec) or with BACE1/ADAM10 5′UTR for 24 h, followed by CNP (100 ng/mL) or DMSO (CTRL) treatment for 24 h, and the relative luciferase activity was normalized to that in CTRL with Vec. Data are expressed as mean ± SEM, **P* < 0.05, ***P* < 0.01, ns: nonsignificant.

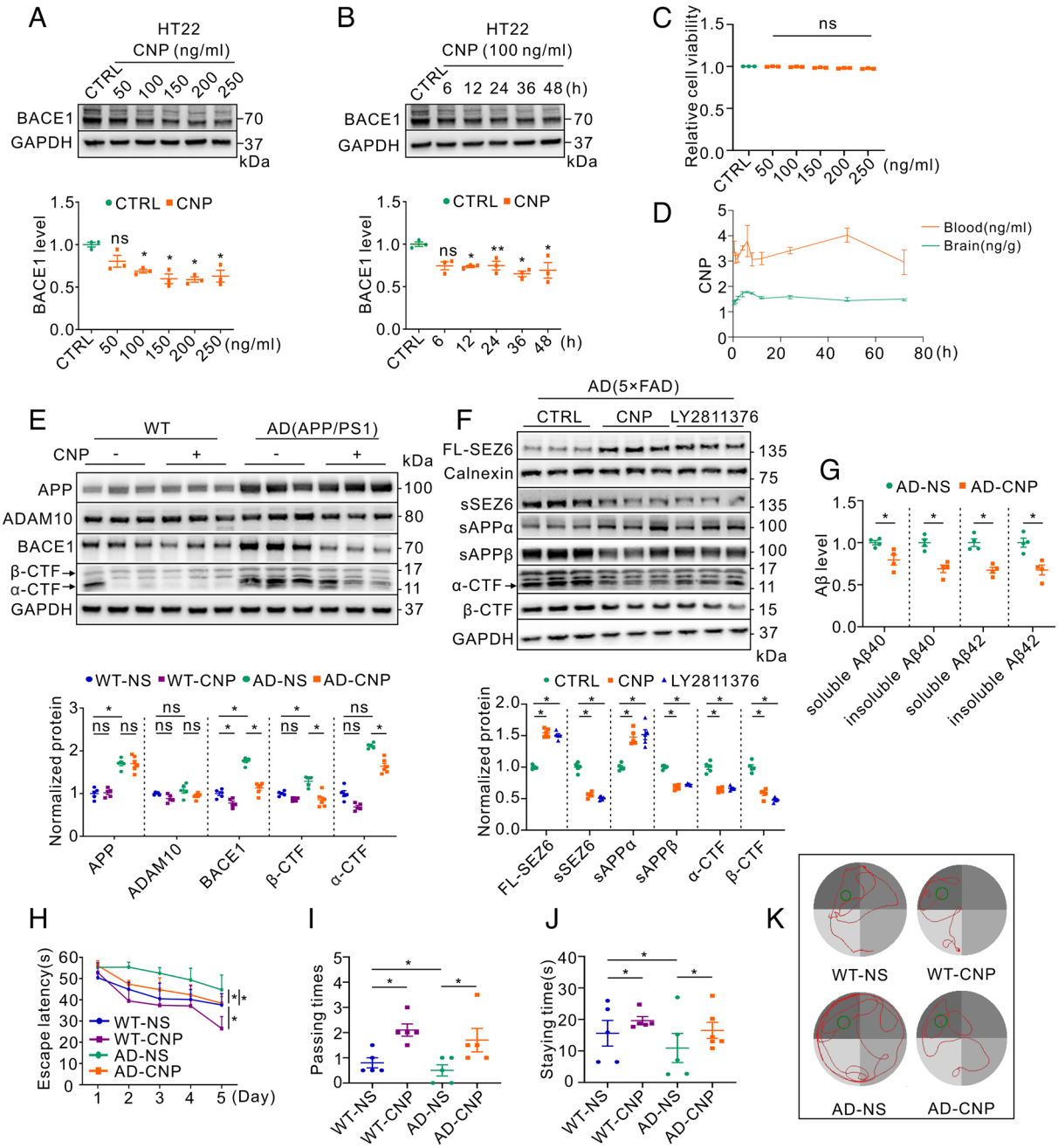

Fig. 2. CNP inhibits amyloidogenesis and rescues cognitive decline in APP/PS1 mice. (*A* and *B*) Dose–response (*A*) and time-course effect (*B*) of CNP on BACE1 protein levels in HT22 cells. BACE1 antibody: Abcam, ab108394. (*C*) Relative cell viability of HT22 cells treated with CNP (0 to 250 ng/mL) for 24 h. (*D*) CNP concentrations in the blood and brain homogenates of mice at 0.5, 1, 2, 4, 6, 8, 12, 24, 48, and 72 h after i.p. injection (10 μg/kg). (*E*) Representative western blots (*Top*) and quantification (*Bottom*) of APP, ADAM10, BACE1, α/β-CTF levels in the hippocampus of male WT and APP/PS1mice (10 mo old), in the absence or presence of CNP (1 μg/kg, i.p.) every other day for 2 mo. Antibody information: APP and α/β-CTF (Sigma, A8717), ADAM10 (Abcam, ab124695), BACE1 (Abcam, ab108394). (*F*) Representative western blots (*Top*) and quantification (*Bottom*) of full-length (FL-SEZ6) and soluble (sSEZ6) SEZ6, sAPPα/β, and α/β-CTFs, in the hippocampus of male 5×FAD mice (3 mo old) i.p. injected with vehicle (normal saline, CTRL), CNP (10 μg/kg), or BACE1 inhibitor LY2811376 (10 mg/kg) for five consecutive days. FL-Sez6 was extracted from membrane fractions and normalized to calnexin, whereas cytosolic proteins were normalized to GAPDH. FL-Sez6/sSez6 (Abcam, ab252863), calnexin (Proteintech, 66903-1-Ig), sAPPα and β-CTF (IBL, 2B3), sAPPβ (BioLegend, SIG-39138), α-CTF (Sigma, A8717). (*G–K*) Wild-type (WT) and APP/PS1 (AD) male mice were i.p. injected with vehicle (normal saline, NS) or CNP (1 μg/kg, every other day) for 2 mo, leading to the following four groups (10 mo old): WT-NS, WT-CNP, AD-NS, and AD-CNP, respectively. (*G*) Soluble and insoluble Aβ40 and Aβ42 species were measured by ELISA in the hippocampus. (*H*) AD mice exhibit a longer escape latency compared to WT mice, whereas CNP-treated mice exhibit a shorter escape latency compared to NS-treated mice in both WT and AD groups. (*I* and *J*) Passing times (*I*) and the staying time (*J*) in the target quadrant by different groups of mice. (*K*) Representative trajectory maps for four groups of mice in the probe trial. Data are expressed as mean ± SEM, $^{*}P < 0.05$, $^{**}P < 0.01$, ns: nonsignificant.

microglial and astrocytic activations are frequently associated with the cytotoxic effect of Aβ (35, 36), we further assessed the activation of microglia and astrocyte by the corresponding markers IBA1 and GFAP. As shown in Fig. 3*J*, the intensity of IBA1 and GFAP was significantly reduced by CNP or shARL. However, CNP failed to reduce IBA1 and GFAP intensity in the presence of shARL, indicating that ARL6IP1 mediated the effect of CNP on AD-like pathology.

The subsequent behavioral testing showed that in the open-field testing, the total traveling distance and the time spent in the central compartment were not significantly different among the tested groups (Fig. 4 *A* and *B*), ruling out the potential influences of

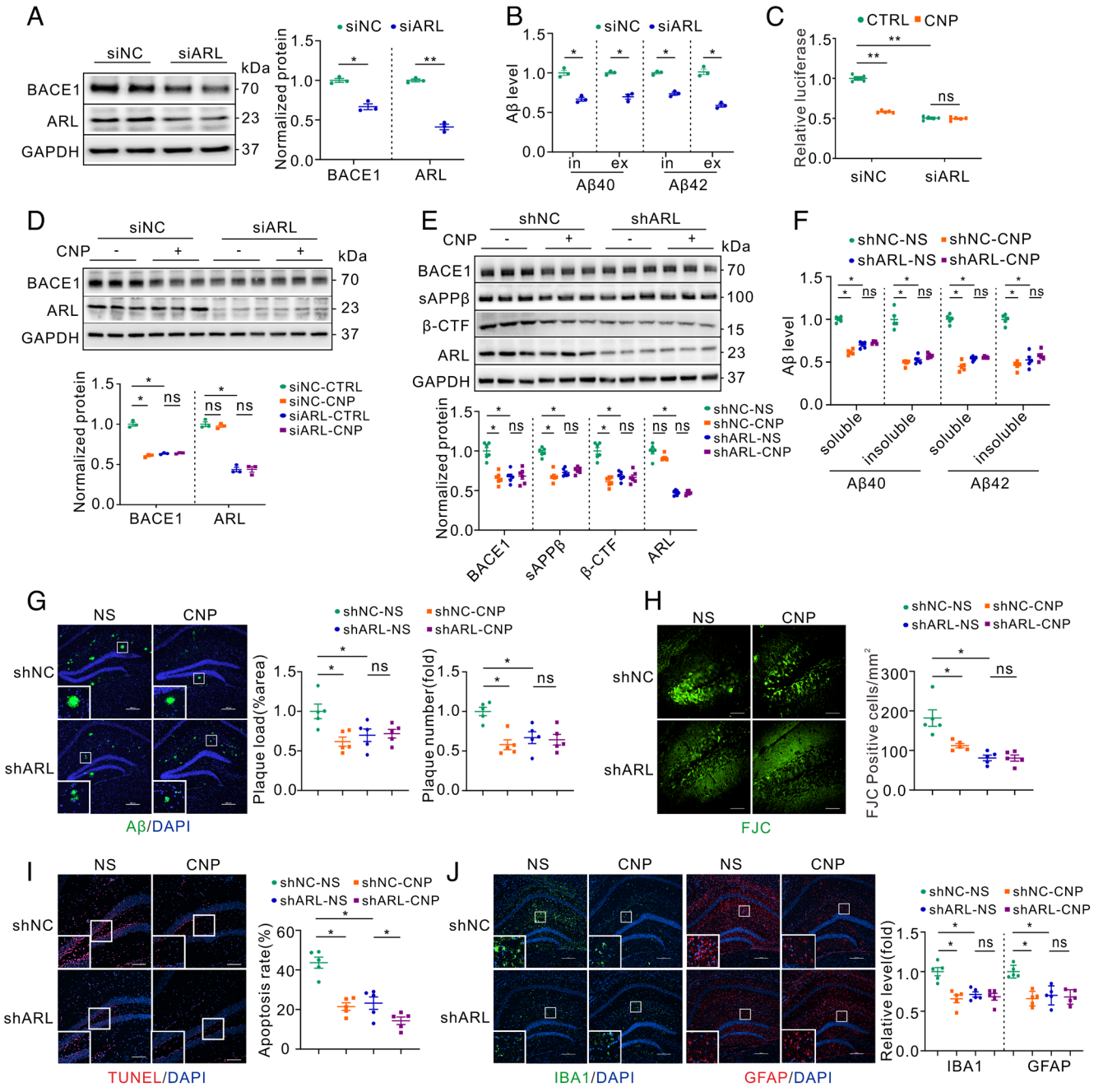

Fig. 3. ARL6IP1 mediates CNP-induced amelioration of AD-like pathologies in APP/PS1 mice. (*A*) Representative western blots (*Left*) and quantification (*Right*) of BACE1 in SH-SY5Y cells transiently transfected with siARL or scrambled (siNC), respectively. Antibody information: BACE1 (Abcam, ab108394), ARL6IP1 (Abcam, ab24228). (*B*) Aβ40 and Aβ42 levels in cell lysates (intracellular, in) and culture medium (extracellular, ex) were measured by ELISA from SH-SY5Y cells transiently transfected with siARL or siNC, respectively. (*C*) Relative luciferase activity of the 5′UTR of BACE1 in SH-SY5Y cells transiently transfected with siNC or siARL for 24 h, in the absence (CTRL) or presence of CNP (100 ng/mL) for further 24 h. (*D*) Representative western blots (*Top*) and quantification (*Bottom*) of BACE1 in SH-SY5Y cells transiently transfected with siARL or siNC for 24 h followed by CNP (100 ng/mL) or DMSO (CTRL) incubation for further 24 h. Antibody information: BACE1 (Abcam, ab108394), ARL6IP1 (Abcam, ab24228). (*E–J*) The hippocampus of male APP/PS1 mice (6 mo old) was bilaterally injected with AAV-shARL6IP1 (shARL) or AAV-shNC, and 4 wk later, mice were i.p. injected with vehicle (normal saline, NS) or CNP (10 μg/kg, every other day) for 2 more months, leading to the following four groups (9 mo old): shNC-NS, shNC-CNP, shARL-NS, and shARL-CNP, respectively. (*E*) Representative western blots (*Top*) and quantification (*Bottom*) of BACE1, sAPPβ, β-CTF, and ARL6IP1(ARL) levels in the hippocampus. Antibody information: BACE1 (Abcam, ab108394), sAPPβ (BioLegend, SIG-39138), β-CTF (IBL, 2B3), ARL6IP1 (Santa Cruz Biotechnology, sc-514476). (*F*) Soluble and insoluble Aβ40 and Aβ42 species were measured by ELISA in the hippocampus. (*G*) Immunofluorescent labeling (*Left*) and quantification (*Right*) of Aβ (green) deposits. DAPI: nucleic marker (blue). (Scale bar: 200 μm.) Aβ antibody: 4G8, BioLegend. (*H*) Representative images (*Left*) and quantification (*Right*) of Fluoro-Jade C (FJC, green)-stained cells in the hippocampus. (Scale bar: 50 μm.) (*I*) Representative images (*Left*) and quantification (*Right*) of TUNEL staining in the hippocampus. (Scale bar: 100 μm.) (*J*) Immunofluorescent labeling (*Left*) and quantification (*Right*) of IBA1 (microglia, green) and GFAP (astrocytes, red). (Scale bar: 200 μm.) Antibody information: IBA1 (GeneTex, GTX632426), GFAP (Proteintech, 60190-1-Ig). Data are expressed as mean ± SEM, $^{*}P < 0.05$, $^{**}P < 0.01$, ns: nonsignificant.

locomotor activity and anxiety on the readout of the subsequent Morris water testing. As shown in Fig. 4*C*, the escape latency was significantly shortened by CNP (shNC-CNP vs. shNC-NS) or shARL (shARL-NS vs. shNC-NS), respectively; whereas no significant differences were found between CNP and shARL (shARL-CNP vs. shARL-NS). Similarly, the passing times and the staying time in the central compartment were significantly altered by CNP in vector control (shNC) but not in shARL (Fig. 4 *D–F*).

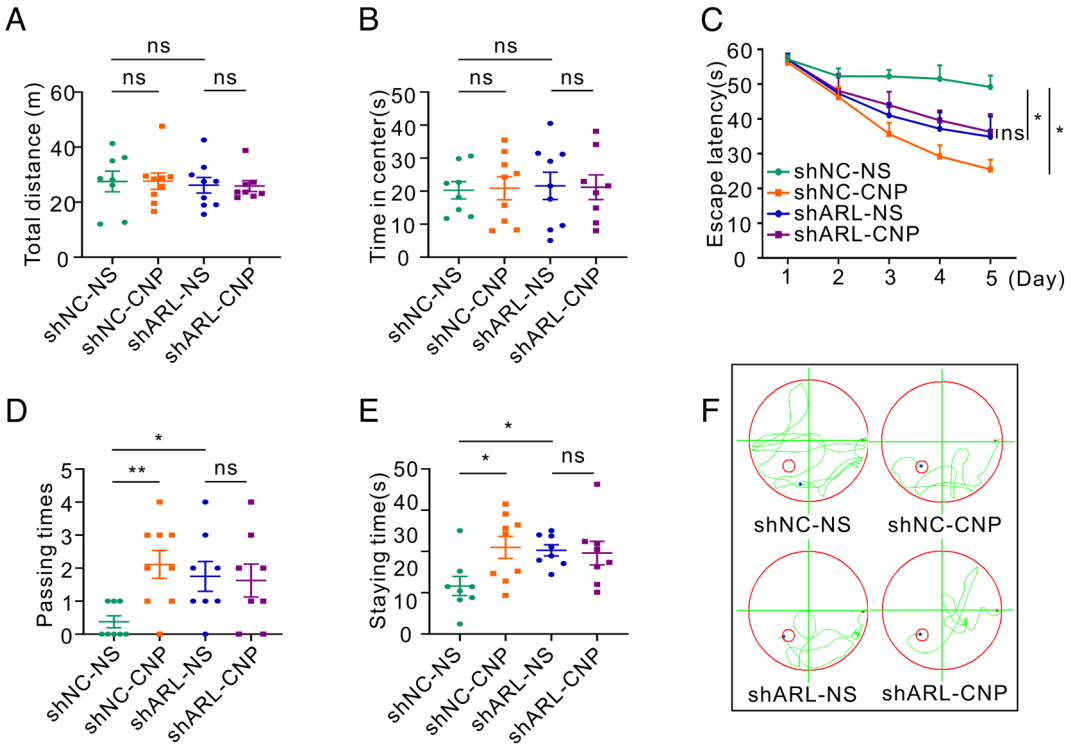

Fig. 4. ARL6IP1 mediates CNP-induced rescue of cognitive decline in APP/PS1 mice. (*A* and *B*) In the open-field task, the total distance traveled (*A*) and the time spent in the center compartment (*B*) between shNC-NS, shNC-CNP, shARL-NS, and shARL-CNP are not significantly different, ruling out the effect of locomotor activity and anxiety on the readout of the Morris water maze test. (*C*–*F*) Quantifications of escape latency (*C*), the passing times (*D*), and staying time (*E*) in the four groups, indicating that the learning and memory performances are affected by ARL6IP1 knockdown, which further prevents the effect of CNP. The representative trajectory maps in the probe trial are shown in *F*. Data are expressed as mean ± SEM, $*P < 0.05$, $**P < 0.01$, ns: nonsignificant.

These results indicated that ARL6IP1 mediated CNP-induced effect on cognitive performances.

ARL6IP1 Interacted with the 5′UTR-Targeted FXR1 in BACE1 Translation. Given that the 5′UTR was critical in BACE1 translation regulated by ARL6IP1 and CNP, we speculated that the 5′UTR-targeted RNA-binding proteins (RBPs) might be associated with the downstream signaling of ARL6IP1. Thus, we next assessed the 5′UTR-targeted RBPs by RNA pulldown combined with liquid chromatography with tandem mass spectrometry (LC-MS/MS) (37). The 5′UTR was labeled by 5-bromo-UTP (BrU) and in vitro transcribed, which was recognized by the anti-BrU antibody and pulled down for protein separation (Fig. 5*A*). A total of 360 and 22 common RBPs were found in two and three biological replications, respectively (Dataset S1). Bioinformatics analysis revealed that these RBPs were closely associated with neurodegenerative diseases including AD, ribosomal proteins, and mRNA processing (*SI Appendix*, Fig. S5), supporting the functional relevance of the 5′UTR in the translation initiation of BACE1.

To identify the potential RBPs that contributed to CNP/ARL6IP1-induced BACE1 translation, we first searched the RBPs that could be altered by CNP in gene expression, through analysis of differentially expressed genes (DEGs) in SH-SY5Y cells that stably overexpress human full-length and neuron-type APP695 (SH-SY5Y-APP) incubated with CNP, which was reminiscent of cellular Aβ overload (38). Among the DEGs (Dataset S2 and *SI Appendix*, Fig. S6), some were indeed overlapped with the 5′UTR-targeted RBPs that included pyridoxal phosphatase (PDXP), H1 histone family member X (H1FX), and enoyl-CoA delta isomerase 1 (ECI1) (*SI Appendix*, Fig. S6*E*). However, although knockdown of these genes successfully altered the basal protein level of BACE1, none of them prevented CNP-induced reduction of BACE1 protein (*SI Appendix*, Fig. S7). Thus, it was unlikely that the DEG-associated RBPs were involved in the regulation of BACE1 translation by CNP.

The alternative mode could be that the potential RBPs mediate the CNP effect by protein–protein interactions (PPIs) with ARL6IP1. Through the online String software analysis, we found that FXR1, FXR2, and DEAD-Box Helicase 17 (DDX17) were common in three biological repeats and were closely interacted (Fig. 5*B*), and all of them were shown to bind to the 5′UTR by RNA pull-down assay (Fig. 5*C*). Interestingly, FXR1/FXR2 was predicted to interact with ARL6IP1 (http://www.cs.utoronto.ca/~juris/data/fpclass/) (39). The subsequent Co-IP results showed that ARL6IP1 coimmunoprecipitated with FXR1/FXR2 but not DDX17 or FMR1 that is known to interact with FXR1/FXR2 (40) (Fig. 5 *D* and *E*). However, whereas knockdown of FXR1 (*SI Appendix*, Fig. S8) or FXR2 led to a decreased protein level at basal condition, silencing of FXR1, but not FXR2, prevented CNP-induced reduction of BACE1 (Fig. 5 *F* and *G*), indicating that FXR1, but not FXR2, was critical in ARL6IP1-mediated regulation of BACE1 translation. Indeed, silencing of FXR1 significantly inhibited the basal level and further prevented CNP-induced reduction of the 5′UTR-luciferase activity (Fig. 5*H*), suggesting that the selective interaction of ARL6IP1 with FXR1 was involved in the regulation of the 5′UTR activity by CNP.

CNP Promoted the Interaction of ARL6IP1 with FXR1 but Inhibited FXR1–5′UTR Binding in Human Cells. It was interesting to note that the protein levels of ARL6IP1 and FXR1 were not dramatically altered by CNP (Figs. 3*E* and 5*G*). We speculated that the reduced BACE1 translation by CNP was through alternative protein–protein and protein–5′UTR (RNA) interactions. Thus,

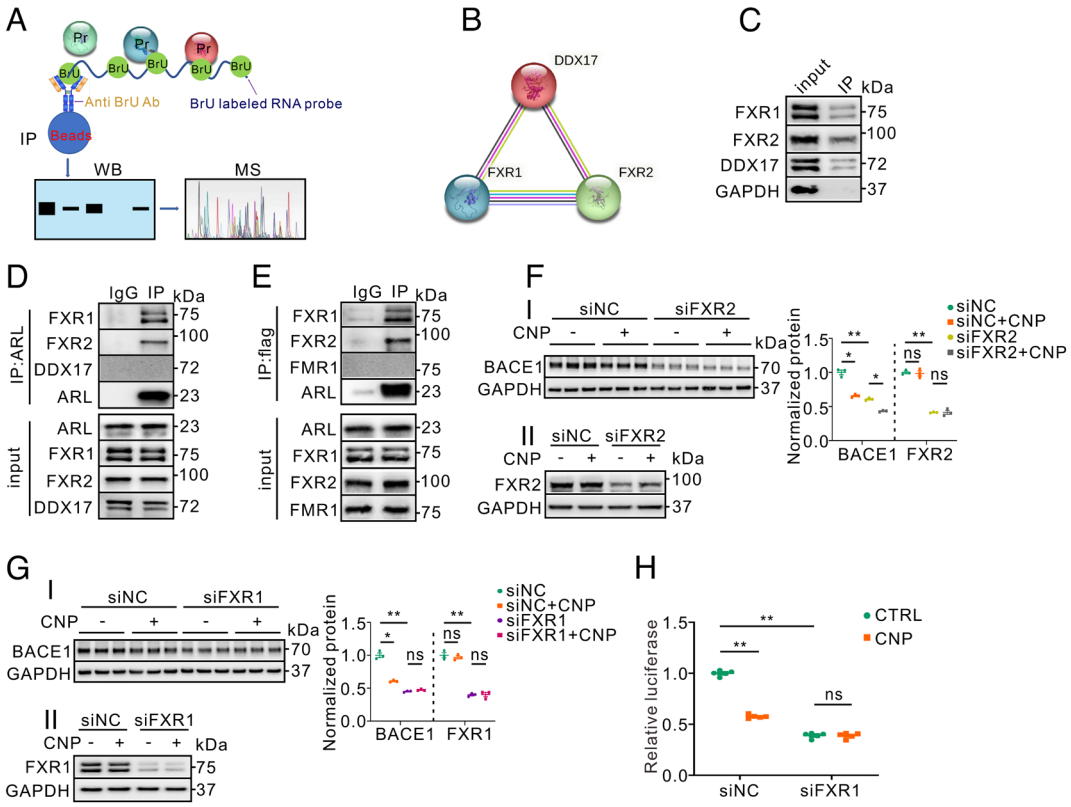

Fig. 5. ARL6IP1 interacts with the 5′UTR-targeted RBP FXR1. (*A*) Schematic diagram for the RNA pulldown combined with MS assay. 5-bromo-UTP (BrU) was randomly incorporated into the 5′UTR upon in vitro transcription. The BrU-labeled 5′UTR was mixed with cell lysates and pulled-down by BrU antibody for subsequent MS analysis. (*B*) The BACE1 5′UTR-targeted RBPs FXR1, FXR2, and DDX17 are interacted with each other, analyzed by online STRING software. (*C*) Representative western blots of FXR1, FXR2, DDX17, and GAPDH in immunoprecipitated extracts by RNA (BACE1 5′UTR) pull-down assay in SH-SY5Y cells. Antibody information: FXR1 (Abcam, ab129089), FXR2 (Proteintech, 12552-1-AP), DDX17 (Abcam, ab180190), GAPDH (Proteintech, 60004-1-Ig). (*D*) Representative western blots of FXR1, FXR2, and DDX17 in immunoprecipitated extracts by ARL6IP1(ARL) antibody in SH-SY5Y cells. Antibody information: FXR1 (Abcam, ab129089), FXR2 (Proteintech, 12552-1-AP), DDX17 (Abcam, ab180190), ARL6IP1 (Abcam, ab24228). (*E*) Representative western blots of FXR1, FXR2, and FMR1 in immunoprecipitated extracts by flag antibody in SH-SY5Y cells transiently transfected with the 3×flag-ARL6IP1 plasmid for 72 h. Antibody information: FXR1 (Abcam, ab129089), FXR2 (Proteintech, 12552-1-AP), FMR1 (Abcam, ab259335), ARL6IP1 (Abcam, ab24228). (*F*) Representative western blots of BACE1 (*i*) and FXR2 (*ii*), and the quantification (*Right*) in SH-SY5Y cells transfected with FXR2 siRNA (siFXR2) or siNC for 24 h, followed by CNP (100 ng/mL) or DMSO (CTRL) treatment for further 24 h. Antibody information: BACE1 (Abcam, ab108394), FXR2 (Proteintech, 12552-1-AP). (*G*) Representative western blots of BACE1 (*i*) and FXR1 (*ii*), and the quantification (*Right*) in SH-SY5Y cells transfected with FXR1 siRNA (siFXR1) or siNC for 24 h, followed by CNP (100 ng/mL) or DMSO (CTRL) treatment for further 24 h. Antibody information: BACE1 (Abcam, ab108394), FXR1 (Abcam, ab129089). (*H*) Relative BACE1 5′UTR-luciferace activity in SH-SY5Y cells transfected with siFXR1 or siNC for 24 h, followed by CNP (100 ng/mL) or DMSO (CTRL) for 24 h. Data are expressed as mean ± SEM, **P* < 0.05, ***P* < 0.01, ns: nonsignificant.

we assessed ARL6IP1 interaction with FXR1 in SH-SY5Y cells treated with CNP. As shown in Fig. 6*A*, the abundance of FXR1 in ARL-precipitated fraction and conversely that of ARL in FXR1-precipitated fraction were significantly enhanced in CNP-treated cells. The augmented interaction between ARL6IP1 and FXR1 was then confirmed by additional immunofluorescent images (Fig. 6*B*). In comparison, colocalization of ARL6IP1 with FXR2 was not altered by CNP (Fig. 6*B*). To visualize the 5′UTR in cells, we first cloned the 5′UTR into the recently developed VN-dEcCas6-VC plasmid, which allowed Cas6-based fluorescence complementation (Cas6FC) to detect target RNAs (41). As shown in Fig. 6*C*, although the Venus-labeled 5′UTR could be clearly visualized, the green signals were relatively week that the colocalization with FXR1 was barely detectable. Thus, we alternatively used the MS2–MS2 phage coat protein (MCP) RNA tracking system (42). As shown in Fig. 6*D*, the MCP-labeled GFP could be clearly visualized and quantified, and the colocalization of GFP with FXR1 allowed to measure the potential binding of the 5′UTR with FXR1, which was significantly decreased in cells treated with CNP. To further verify this, RNA immunoprecipitation (RIP) combined with RT-qPCR showed that the BACE1 mRNA that bound to FXR1 was significantly reduced in CNP-treated cells (Fig. 6*E*), indicating that CNP reduced FRX1–5′UTR interaction in human cells.

CNP Enhanced ARL6IP1–FXR1 Interaction and Inhibited FXR1–5′UTR Binding in Murine Cells. To further confirm that CNP-mediated regulation of BACE1 in mice was through the same mechanism as in human cells, we assessed the interaction between ARL6IP1 and FXR1 in murine cells. RNA pull-down assay showed that FXR1 could bind to the 5′UTR in HT22 cells (Fig. 7*A*), and the interaction of ARL6IP1 with FXR1 was significantly increased by either ARL- or FXR1-probed immunoprecipitation (Fig. 7*B*). To assess the alteration of FXR1–5′UTR binding in mice, we used in utero electroporation which mediated the transfer of MS2–MCP system into the brain. As shown in Fig. 7*C*, the GFP-coupled MCP was clearly visualized, which could be colocalized with FXR1 in the brain slices, indicating a successful gene transfection. In CNP-treated mice, the colocalization between FXR1 and the 5′UTR was significantly reduced. These results indicated that the dynamic interaction of ARL6IP1–FXR1–5′UTR occurred in human and murine cells treated with CNP, which could be responsible for the inhibition of BACE1 translation and Aβ generation (Fig. 7*D*).

Discussion

RNA–protein interactions are not static but dynamically regulated (43). With advances in technology, it is reported that the dynamic RBP–RNA binding occurs during translational arrest and

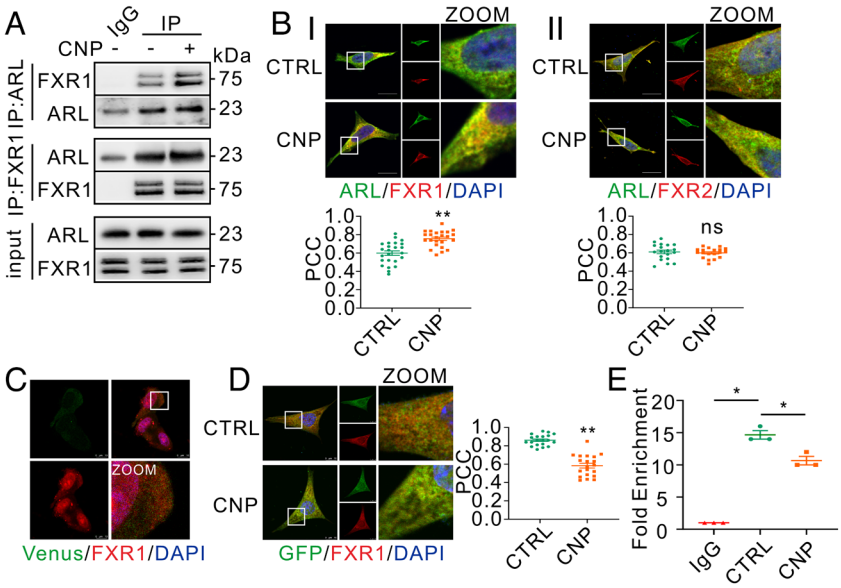

Fig. 6. CNP promotes ARL6IP1–FXR1 interaction but inhibits FXR1–5′UTR binding in human cells. (*A*) Western blots show FXR1 that is coimmunoprecipitated with ARL6IP1 (ARL, *Top*), or ARL that is coimmunoprecipitated with FXR1 (*Middle*) is enhanced in SH-SY5Y cells treated with CNP (100 ng/mL) for 24 h, whereas the protein level of ARL and FXR1 in input is not significantly altered (*Bottom*). Antibody information: FXR1 (Abcam, ab129089), ARL6IP1 (Abcam, ab24228). (*B*) Immunofluorescent images show the colocalization of ARL with FXR1 (*i*) or FXR2 (*ii*) in SH-SY5Y cells treated with CNP (100 ng/mL) or DMSO (CTRL) for 24 h. (Scale bar: 25 μm.) PCC: Pearson's correlation coefficient. Antibody information: ARL6IP1 (GeneTex, GTX85516), FXR1 (Santa Cruz Biotechnology, sc-374148), FXR2 (Santa Cruz Biotechnology, sc-32266). (*C*) Immunofluorescent images of Venus (green, autofluorescence) and FXR1 (red) in SH-SY5Y cells cotransfected with BACE1 5′UTR-8xCBS and VN-dEcCas6-VC plasmid for 48 h. (Scale bar: 10 μm.) FXR1 antibody: Santa Cruz Biotechnology, sc-374148. (*D*) Representative immunofluorescent images (*Left*) and quantification (*Right*) of the colocalization between FXR1 (red) and the 5′UTR-labeled GFP (green, autofluorescence), in SH-SY5Y cells cotransfected with MS2-BACE1 5′UTR and MCB-GFP plasmid for 24 h, with CNP (100 ng/mL) or DMSO (CTRL) treatment for further 24 h. (Scale bar: 10 μm.) FXR1 antibody: Santa Cruz Biotechnology, sc-374148. (*E*) Relative BACE1 mRNA levels measured by RT-qPCR in cell extracts immunoprecipitated by FXR1 or IgG antibody. SH-SY5Y cells were treated with CNP (100 ng/mL) or DMSO (CTRL) for 24 h. Data are expressed as mean ± SEM, $*P < 0.05$, $**P < 0.01$. ns: nonsignificant.

correlates with cellular functions of RBPs (44, 45). Although alterations of RBPs are one of the prominent features of AD (46), how RBP might be involved in the pathogenesis of AD is not completely understood. In our study, the reduced interaction of FXR1 with the 5′UTR underlies CNP-induced inhibition of BACE1 translation, providing evidence that the FXR1 functions as RBP that directly regulates amyloidogenesis. As the protein levels of FXR1 and ARL6IP1 are not altered by CNP, the dynamic nature of RNA–protein interactions expands our understating of disease mechanisms inspired by large-scale genomics and proteomics studies (47–49).

BACE1 protein and activity are increased in the brain of AD (50). It is reported that BACE1 translation is inhibited by the presence of the 5′UTR (51). The 5′UTR activity could be regulated by cis-elements especially upstream of AUGs (52, 53), and a variety of factors including double-stranded RNA-activated protein kinase, E3 ligase CHIP, eukaryotic initiation factors 2α and 4B, and translation elongation factor Tu of mitochondria (23, 54–57), highlighting an important role of BACE1 translation in the pathophysiology of AD (58). In our study, CNP seems to inhibit Aβ generation by preferentially reducing the protein of BACE1 relative to APP and ADAM10 in cultured cells and the brain of APP/PS1 mice. Moreover, the following evidence supports that CNP reduces BACE1 protein through the 5′UTR-dependent translation: BACE1 mRNA is not altered; the inhibitor of translation but not transcription, proteosome, and lysosome blocks this effect; and CNP directly inhibits the 5′UTR-luciferase activity. As CNP reaches the brain quickly, it is not surprising that the cognitive deficits of APP/PS1 are improved.

BACE1 inhibition consistently increases sAPPα level in mice and humans (59–61). Similarly, α-CTF, the intracellular fragment of APP catalyzed by ADAM10, is also elevated in primary neurons and brain by BACE1 inhibition (31, 62). However, α-CTF can be decreased under some conditions. In 5×FAD mice, BACE1 haploinsufficiency or inhibition causes a reduction of α-CTF, with sAPPα being increased or unchanged (61, 63), and loss of BACE1 leads to an early increase but late decrease of α-CTF starting at 120 postnatal days (64). Interestingly, enhancement of α-CTF by siBACE1 in cultured neurons could be reversed by APP overexpression (65). In human iPSC-derived neurons with PSEN1 mutation or γ-secretase inhibitor, siBACE1 causes a slight decrease of α-CTF (66). These conditions correlate commonly with an enhanced α- and β-CTF level as a result of APP overexpression or γ-secretase inhibition. Accumulation of intracellular C99, which is more relevant to neuronal damage than Aβ in the brain of AD patients (67), impairs lysosomal proteolysis and mitophagy (68, 69). Thus, reducing C99 from high level could relieve lysosomal inhibition, resulting in an efficient degradation of α-CTF. In line with this, lysosomal inhibitor chloroquine increases α-CTF relative to β-CTF in a dose-dependent manner (70, 71). In our study, CNP, in a similar way to BACE1 inhibitor, reduces β- and α-CTF in the brain of APP/PS1 and 5×FAD mice, which is in agreement with our previous report (23). Whereas sAPPα is significantly increased in animal models, the failure of sAPPα elevation in cultured cells by CNP might be associated with a partial reduction instead of complete loss of BACE1. It is tempting to speculate that depending on experimental conditions and, particularly the basal level of APP/C99, BACE1 inhibition could lead to a reduction of α-CTF.

Although gene mutation or knockout of ARL6IP1 causes spastic paraplegia or developmental delay (20, 22), ARL6IP1 KD significantly inhibits BACE1 expression, Aβ level, and neurodegeneration in the current study, suggesting that ARL6IP1 deficiency is rather beneficial for AD. In human cells, ARL6IP1 KD also reduces the 5′UTR-luciferase activity and blocks CNP-induced inhibition of BACE1 translation, indicating that ARL6IP1

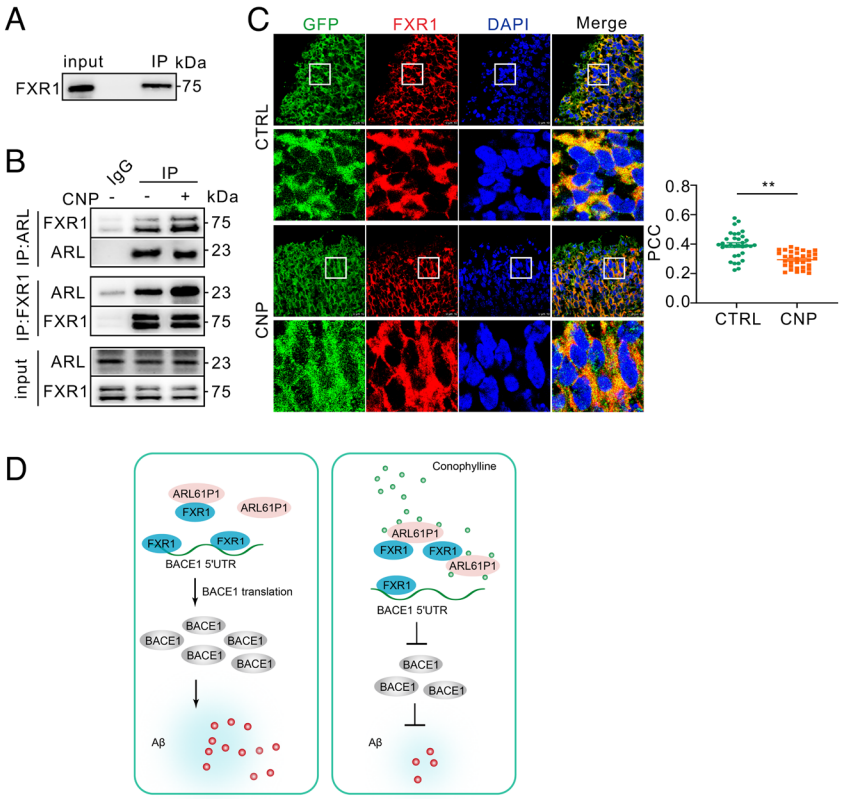

Fig. 7. CNP enhances ARL6IP1–FXR1 interaction and reduces FXR1–5′UTR binding in murine cells. (*A*) Representative western blots of FXR1 in immunoprecipitated extracts by RNA pulldown using BrU-labeled 5′UTR in HT22 cells. FXR1 antibody: Abcam, ab129089. (*B*) Western blots show FXR1 that is coimmunoprecipitated with ARL6IP1 (ARL, *Top*), and ARL that is coimmunoprecipitated with FXR1 (*Middle*) is increased in HT22 cells treated with CNP (100 ng/mL) for 24 h, whereas the protein level of ARL and FXR1 in input is not altered relative to CTRL (*Bottom*). Antibody information: FXR1 (Abcam, ab129089), ARL6IP1 (Santa Cruz Biotechnology, sc-514476). (*C*) Immunofluorescent images (*Left*) and colocalization analysis (*Right*) of the 5′UTR-labeled GFP (green), FXR1 (red), and DAPI (blue) in brain slices cotransfected with MS2-BACE1 5′UTR and MCB-GFP, in the absence (CTRL) or presence of CNP (10 μg/kg). (Scale bar: 10 μm.) FXR1 antibody: Santa Cruz Biotechnology, sc-374148. (*D*) Schematic diagram depicts the dynamic interaction of ARL6IP1–FXR1–5′UTR in the regulation of BACE1 translation by CNP. The enhanced ARL6IP1–FXR1 interaction correlates with the reduced FXR1–5′UTR binding, which contributes to CNP-induced inhibition of BACE1 translation and Aβ generation. Data are expressed as mean ± SEM, $^{**}P < 0.01$.

mediates the effect of CNP through the 5′UTR. Moreover, AAV-mediated delivery of ARL6IP1 shRNA, alone, reduces BACE1 protein level and Aβ load, inhibits microglial and astrocytic activation, and improves cognitive functions in APP/PS1 mice; in the presence of ARL6IP1 shRNA, CNP does not show further effects, supporting that ARL6IP1 is a target molecule of CNP.

Recent evidence has revealed an increased number of RBPs that are involved in human genetic diseases (72). We have established a RBP list by targeting the 5′UTR of BACE1, which should provide a comprehensive source for further understanding of BACE1 translation initiation. As some of the RBPs, including PDXP, H1FX, and ECI1, are changed by CNP in gene expression through DEG analysis, it is possible that these RBPs could contribute to CNP-induced BACE1 regulation. However, despite that silencing of the individual RBPs alters BACE1 protein level, CNP-induced reduction of BACE1 is not affected (*SI Appendix*, Fig. S7). Thus, CNP may alternatively use ARL6IP1 to link to the potential RBPs that are not altered in gene expression. Indeed, by excluding DDX17 and FXR2, the involvement of FXR1 in mediating the function of ARL6IP1 is supported by the following findings: FXR1 is coimmunoprecipitated and colocalized with ARL6IP1, this interaction is enhanced by CNP, and silencing of FXR1 inhibits 5′UTR-luciferase activity and prevents CNP-induced reduction of BACE1. We speculate that the protein–protein interaction between ARL6IP1 and FXR1 plays an important role in BACE1 translation that is regulated by CNP.

FXR1 controls synaptic plasticity through the 5′UTR-dependent mechanism (73). Importantly, FXR1 also colocalizes with Aβ plaques (74), suggesting a close association with amyloidogenesis. The FXR1–RNA interaction is supported by a recent report demonstrating that liquid–liquid phase separation (LLPS) promotes FXR1-activated translation of the stored mRNA (75). The 5′UTR in translation initiation could involve the cap-dependent and -independent mechanisms (76), and the latter involve the so-called cap-independent translation enhancers (CITE) that bind mRNA-recruiting translation machinery such as ribosomal proteins and eIFs (77). In our study, although whether LLPS is involved in the dynamic interaction of FXR1 with the 5′UTR remains to be further investigated, the reduced FXR1–5′UTR binding is correlated with the decreased 5′UTR activity and BACE1 translation, indicating that FXR1 regulates translation initiation of BACE1. Moreover, as the luciferase reporter is designed with an uncapped sequence of the 5′UTR, the significantly reduced luciferase activity by FXR1 KD suggests an involvement of CITE mechanism. In line with this, many translation initiation components including eIFs and RNA helicases are found in the 5′UTR-targeted RBPs (Dataset S1), which might cooperate with FXR1 to regulate the 5′UTR activity.

We propose a model that CNP exhibits a therapeutic potential for AD by inhibiting BACE1 translation (Fig. 7*D*). Under basal condition, the 5′UTR–FXR1 binding contributes to the maintenance of BACE1 translation; upon CNP treatment, the enhanced ARL6IP–FXR1 interaction promotes the dissociation of FXR1

from the 5′UTR, leading to an inhibition of BACE1 translation, Aβ deposition, and the resulting glial activation, contributing to the rescue of cognitive decline in APP/PS1 mice.

Materials and Methods

Experimental details are included in *SI Appendix, Materials and Methods*.

Animal Work. All mouse generation, husbandry, and experimental procedures were approved by the Commission of Chongqing Medical University for ethics of experiments on animals, in accordance with international standards. APP/PS1 and 5×FAD transgenic mice were purchased from Jackson Laboratory (Nanjing, China). Only male adult mice were included. APP/PS1 mice intraperitoneally (i.p.) injected with CNP in the absence or presence of hippocampi were bilaterally injected shARL6IP1-AAV, followed by behavioral tests. To compare the efficacy, 5×FAD mice were i.p. injected with CNP or LY2811376. To cotransfect with MS2-BACE1 5′UTR and MCB-GFP plasmid, in utero electroporation was performed on pregnant ICR mice (Ensiweier biotech, Chongqing, China). Details of animal treatment and brain sample preparation, behavioral tests, measurement of CNP concentration, and in utero electroporation are included in *SI Appendix, Materials and Methods*.

Cell Culture. SH-SY5Y, HT22, BV-2, U251MG, and SH-SY5Y-APP cells were grown in DMEM containing F12 (DMEM-F12, Gibco) or DMEM (Gibco) with 10% fetal bovine serum (FBS, Gibco) and 1% penicillin/streptomycin (Beyotime Biotechnology) at 37 °C under 5% CO_2 and 95% O_2.

WB, CO-IP. Denatured protein samples were separated by 8% SDS-PAGE gels, and a specific 16.5% Tris-tricine gel was used for CTF detection. For CO-IP, cell extracts were incubated with antibodies that were coupled with Protein A/G beads (MedChemExpress, HY-K0202), and the resultant IP pellets were detected by WB.

RNA Pulldown, RIP, and RT-qPCR. RNA pull-down assay was performed according to the protocol of RiboTrap Kit (MBL International). RIP assays were performed using Magna RIP RNA-binding protein immunoprecipitation kit (Millipore). For RT-qPCR, total RNA was extracted using RNAiso plus kit (Takara), and cDNA was generated with the reverse transcriptase kit (R233-01-AC, Vazyme). The BACE1 mRNA level was detected using SYBR Green PCR Master Mix kit (Q711-02/03, Vazyme) with Bio-Rad IQ5 detection system (Bio-Rad).

Biochemical Assays. Cell viability was measured by using CCK-8 Cell Counting Kit (MedChemExpress), Aβ1-40 and Aβ1-42 were measured by using ELISA kit (Elabscience, E-EL-H0542c, E-EL-H0543c), and luciferase activity was measured by using Luciferase Reporter Gene Assay Kit (Beyotime Biotechnology, RG089S/RG042S), according to the manufacturer's instructions.

Pathological Techniques. Immunohistochemistry was performed by using immunohistochemical test kit (PV-9002, ZSGB-BIO), FJC staining was performed by using Fluoro-Jade C staining Kit (Biosensis, TR-100-FJ), and TUNEL staining was performed by using One-Step TUNEL Apoptosis Assay Kit (Meilunbio, MA0224), according to the manufacturer's instructions.

Statistical Analysis. All data were analyzed with GraphPad Prism9 (GraphPad Software) and shown as mean ± SEM. The statistical comparisons between the two groups were tested using Student's *t* test. The comparisons among groups were tested using one-way or two-way ANOVA. Statistical significance was achieved at $P < 0.05$.

Data, Materials, and Software Availability. All study data are included in the article and/or *SI Appendix*.

ACKNOWLEDGMENTS. We sincerely thank Dr. C. -Y. Han at Hebei University of Science and Technology for providing VN-dEcCas6-VC and actin-8×CBS plasmids. This work was supported by NSFC (81971030, 82271461) and Chongqing Education commission (KJZD-K201900404) to G.-J.C.

Author affiliations: [a]Department of Neurology, the First Affiliated Hospital of Chongqing Medical University, Chongqing Key Laboratory of Major Neurological and Mental Disorders, Chongqing Key Laboratory of Neurology, 1 Youyi Road, Chongqing 400016, China; [b]Center for Novel Target & Therapeutic Intervention, Institute of Life Sciences, Chongqing Medical University, Chongqing 400016, China; [c]Institute for Brain Science and Disease, Chongqing Medical University, Chongqing 400016, China; and [d]State Key Laboratory of Phytochemistry and Plant Resources in West China, Kunming Institute of Botany, Chinese Academy of Sciences, Kunming 650201, China

1. J. Cummings *et al.*, Alzheimer's disease drug development pipeline: 2022. *Alzheimers Dement. (N Y)* **8**, e12295 (2022).
2. J. Cummings, N. Fox, Defining disease modifying therapy for Alzheimer's disease. *J. Prev. Alzheimers Dis.* **4**, 109–115 (2017).
3. P. Scheltens *et al.*, Alzheimer's disease. *Lancet* **397**, 1577–1590 (2021).
4. J. Weller, A. Budson, Current understanding of Alzheimer's disease diagnosis and treatment. *F1000Res* **7**, 1161 (2018).
5. R. Nativio *et al.*, An integrated multi-omics approach identifies epigenetic alterations associated with Alzheimer's disease. *Nat. Genet.* **52**, 1024–1035 (2020).
6. B. Bai *et al.*, Deep multilayer brain proteomics identifies molecular networks in Alzheimer's disease progression. *Neuron* **105**, 975–991.e7 (2020).
7. M. Wang *et al.*, Transformative network modeling of multi-omics data reveals detailed circuits, key regulators, and potential therapeutics for Alzheimer's disease. *Neuron* **10**, 257–272.e14 (2021).
8. R. Yan *et al.*, Membrane-anchored aspartyl protease with Alzheimer's disease beta-secretase activity. *Nature* **402**, 533–537 (1999).
9. R. Vassar *et al.*, Beta-secretase cleavage of Alzheimer's amyloid precursor protein by the transmembrane aspartic protease BACE. *Science* **286**, 735–741 (1999).
10. M. F. Egan *et al.*, Randomized trial of verubecestat for prodromal Alzheimer's disease. *N. Engl. J. Med.* **380**, 1408–1420 (2019).
11. M. Hrabinova *et al.*, Is it the twilight of BACE1 inhibitors? *Curr. Neuropharmacol.* **19**, 61–77 (2021).
12. B. Das *et al.*, BACE1 controls synaptic function through modulating release of synaptic vesicles. *Mol. Psychiatry* **26**, 6394–6410 (2021).
13. L. Chami, F. Checler, BACE1 is at the crossroad of a toxic vicious cycle involving cellular stress and β-amyloid production in Alzheimer's disease. *Mol. Neurodegener* **7**, 52 (2012).
14. H. W. Querfurth, F. M. LaFerla, Alzheimer's disease. *N. Engl. J. Med.* **362**, 329–344 (2010).
15. Y. Yamamoto, A. Yoshida, N. Miyazaki, K. Iwasaki, T. Sakisaka, Arl6IP1 has the ability to shape the mammalian ER membrane in a reticulon-like fashion. *Biochem. J.* **458**, 69–79 (2014).
16. R. Dong *et al.*, The inositol 5-phosphatase INPP5K participates in the fine control of ER organization. *J. Cell Biol.* **217**, 3577–3592 (2018).
17. P. Fowler, N. O'Sullivan, ER-shaping proteins are required for ER and mitochondrial network organization in motor neurons. *Hum. Mol. Genet.* **25**, 2827–2837 (2016).
18. M. Nizon *et al.*, ARL6IP1 mutation causes congenital insensitivity to pain, acromutilation and spastic paraplegia. *Clin. Genet.* **93**, 169–172 (2018).
19. S. Wakil *et al.*, Truncating ARL6IP1 variant as the genetic cause of fatal complicated hereditary spastic paraplegia. *BMC Med. Genet.* **20**, 119 (2019).
20. S. Maddirevula *et al.*, Autozygome and high throughput confirmation of disease genes candidacy. *Genet. Med.* **21**, 736–742 (2019).
21. H. Huang *et al.*, The embryonic expression patterns and the knockdown phenotypes of zebrafish ADP-ribosylation factor-like 6 interacting protein gene. *Dev. Dyn.* **238**, 232–240 (2009).
22. C. Tu, T. Yang, H. Huang, H. Tsai, Zebrafish arl6ip1 is required for neural crest development during embryogenesis. *PLoS One* **7**, e32899 (2012).
23. B. L. Zhu *et al.*, MMP13 inhibition rescues cognitive decline in Alzheimer transgenic mice via BACE1 regulation. *Brain* **142**, 176–192 (2019).
24. Z. Min *et al.*, Cosmosiin increases ADAM10 expression via mechanisms involving 5′UTR and PI3K signaling. *Front. Mol. Neurosci.* **11**, 198 (2018).
25. K. Umezawa *et al.*, Therapeutic activity of plant-derived alkaloid conophylline on metabolic syndrome and neurodegenerative disease models. *Hum. Cell* **31**, 95–101 (2018).
26. T. Yamanaka *et al.*, Conophylline inhibits hepatocellular carcinoma by inhibiting activated cancer-associated fibroblasts through suppression of G protein-coupled receptor 68. *Mol. Cancer Ther.* **20**, 1019–1028 (2021).
27. C. Andrade, Psychotropic drugs with long half-lives: Implications for drug discontinuation, occasional missed doses, dosing interval, and pregnancy planning. *J. Clin. Psychiatry* **83**, 22f14593 (2022).
28. Y. Jiang *et al.*, Partial BACE1 reduction in a Down syndrome mouse model blocks Alzheimer-related endosomal anomalies and cholinergic neurodegeneration: Role of APP-CTF. *Neurobiol. Aging* **39**, 90–98 (2016).
29. P. C. May *et al.*, Robust central reduction of amyloid-β in humans with an orally available, non-peptidic β-secretase inhibitor. *J. Neurosci.* **31**, 16507–16516 (2011).
30. M. Pigoni *et al.*, Seizure protein 6 and its homolog seizure 6-like protein are physiological substrates of BACE1 in neurons. *Mol. Neurodegener.* **11**, 67 (2016).
31. M. H. Ou-Yang *et al.*, Axonal organization defects in the hippocampus of adult conditional BACE1 knockout mice. *Sci. Translational Med.* **10**, eaao5620 (2018).
32. E. Suzuki *et al.*, Preparation of conophylline affinity nano-beads and identification of a target protein. *Bioorganic Med. Chem.* **17**, 6188–6195 (2009).
33. H. Yamaguchi, J. Shen, Histological analysis of neurodegeneration in the mouse brain. *Methods Mol. Biol.* **1004**, 91–113 (2013).
34. A. Ehara, S. Ueda, Application of Fluoro-Jade C in acute and chronic neurodegeneration models: Utilities and staining differences. *Acta Histochem. Cytochem.* **42**, 171–179 (2009).
35. D. V. Hansen, J. E. Hanson, M. Sheng, Microglia in Alzheimer's disease. *J. Cell Biol.* **217**, 459–472 (2018).
36. B. De Strooper, E. Karran, The Cellular phase of Alzheimer's disease. *Cell* **164**, 603–615 (2016).
37. K. Masuda *et al.*, Arid5a controls IL-6 mRNA stability, which contributes to elevation of IL-6 level in vivo. *Proc. Natl. Acad. Sci. U.S.A.* **110**, 9409–9414 (2013).
38. X. Wang *et al.*, Insulin inhibits Abeta production through modulation of APP processing in a cellular model of Alzheimer's disease. *Neuro Endocrinol. Lett.* **35**, 224–229 (2014).
39. M. Kotlyar *et al.*, In silico prediction of physical protein interactions and characterization of interactome orphans. *Nat. Methods* **12**, 79–84 (2015).

40. Y. Zhang *et al.*, The fragile X mental retardation syndrome protein interacts with novel homologs FXR1 and FXR2. *EMBO J.* **14**, 5358–5366 (1995).
41. F. Gao, K. Zheng, Y. B. Li, F. Jiang, C. Y. Han, A Cas6-based RNA tracking platform functioning in a fluorescence-activation mode. *Nucleic Acids Res.* **50**, e46 (2022).
42. J. H. Yoon, M. Gorospe, Identification of mRNA-interacting factors by MS2-TRAP (MS2-tagged RNA affinity purification). *Methods Mol. Biol.* **1421**, 15–22 (2016).
43. D. Licatalosi, X. Ye, E. Jankowsky, Approaches for measuring the dynamics of RNA-protein interactions. *Wiley Interdiscip. Rev. RNA* **11**, e1565 (2020).
44. D. Sharma *et al.*, The kinetic landscape of an RNA-binding protein in cells. *Nature* **591**, 152–156 (2021).
45. J. Trendel *et al.*, The human RNA-binding proteome and its dynamics during translational arrest. *Cell* **176**, 391–403.e19 (2019).
46. A. Rybak-Wolf, M. Plass, RNA dynamics in Alzheimer's disease. *Molecules* **26**, 5113 (2021).
47. E. Johnson *et al.*, Large-scale proteomic analysis of Alzheimer's disease brain and cerebrospinal fluid reveals early changes in energy metabolism associated with microglia and astrocyte activation. *Nat. Med.* **26**, 769–780 (2020).
48. I. Jansen *et al.*, Genome-wide meta-analysis identifies new loci and functional pathways influencing Alzheimer's disease risk. *Nat. Genet.* **51**, 404–413 (2019).
49. B. Kunkle *et al.*, Genetic meta-analysis of diagnosed Alzheimer's disease identifies new risk loci and implicates Aβ, tau, immunity and lipid processing. *Nat. Genet.* **51**, 414–430 (2019).
50. X. Sun, K. Bromley-Brits, W. Song, Regulation of β-site APP-cleaving enzyme 1 gene expression and its role in Alzheimer's disease. *J. Neurochem.* **120**, 62–70 (2012).
51. S. Lammich, S. Schöbel, A. K. Zimmer, S. F. Lichtenthaler, C. Haass, Expression of the Alzheimer protease BACE1 is suppressed via its 5′-untranslated region. *EMBO Rep.* **5**, 620–625 (2004).
52. M. Mihailovich, R. Thermann, F. Grohovaz, M. W. Hentze, D. Zacchetti, Complex translational regulation of BACE1 involves upstream AUGs and stimulatory elements within the 5′ untranslated region. *Nucleic Acids Res.* **35**, 2975–2985 (2007).
53. W. Zhou, W. Song, Leaky scanning and reinitiation regulate BACE1 gene expression. *Mol. Cell. Biol.* **26**, 3353–3364 (2006).
54. P. Picón-Pagès *et al.*, Amyloid beta-peptide increases BACE1 translation through the phosphorylation of the eukaryotic initiation factor-2α. *Oxid. Med. Cell. Longev.* **2020**, 2739459 (2020).
55. B. R. Zhong *et al.*, TUFM is involved in Alzheimer's disease-like pathologies that are associated with ROS. *FASEB J.* **35**, e21445 (2021).
56. G. Ill-Raga *et al.*, Activation of PKR causes amyloid ß-peptide accumulation via de-repression of BACE1 expression. *PLoS One* **6**, e21456 (2011).
57. A. K. Singh, U. Pati, CHIP stabilizes amyloid precursor protein via proteasomal degradation and p53-mediated trans-repression of β-secretase. *Aging Cell* **14**, 595–604 (2015).
58. F. X. Guix, C. L. Sartório, G. Ill-Raga, BACE1 translation: At the crossroads between Alzheimer's disease neurodegeneration and memory consolidation. *J. Alzheimer's Dis. Rep.* **3**, 113–148 (2019).
59. H. Fukumoto *et al.*, A noncompetitive BACE1 inhibitor TAK-070 ameliorates Abeta pathology and behavioral deficits in a mouse model of Alzheimer's disease. *J. Neurosci.* **30**, 11157–11166 (2010).
60. M. Timmers *et al.*, Pharmacodynamics of atabecestat (JNJ-54861911), an oral BACE1 inhibitor in patients with early Alzheimer's disease: Randomized, double-blind, placebo-controlled study. *Alzheimers Res. Ther.* **10**, 85 (2018).
61. L. Devi, M. Ohno, Effects of BACE1 haploinsufficiency on APP processing and Aβ concentrations in male and female 5XFAD Alzheimer mice at different disease stages. *Neuroscience* **307**, 128–137 (2015).
62. D. Dominguez *et al.*, Phenotypic and biochemical analyses of BACE1- and BACE2-deficient mice. *J. Biol. Chem.* **280**, 30797–30806 (2005).
63. L. Devi, J. Tang, M. Ohno, Beneficial effects of the β-secretase inhibitor GRL-8234 in 5XFAD Alzheimer's transgenic mice lessen during disease progression. *Curr. Alzheimer Res.* **12**, 13–21 (2015).
64. X. Hu, B. Das, H. Hou, W. He, R. Yan, BACE1 deletion in the adult mouse reverses preformed amyloid deposition and improves cognitive functions. *J. Exp. Med.* **215**, 927–940 (2018).
65. S. C. Kao, A. M. Krichevsky, K. S. Kosik, L. H. Tsai, BACE1 suppression by RNA interference in primary cortical neurons. *J. Biol. Chem.* **279**, 1942–1949 (2004).
66. D. Kwart *et al.*, A large panel of isogenic APP and PSEN1 mutant human iPSC neurons reveals shared endosomal abnormalities mediated by APP β-CTFs, not Aβ. *Neuron* **104**, 256–270.e5 (2019).
67. M. V. Pulina, M. Hopkins, V. Haroutunian, P. Greengard, V. Bustos, C99 selectively accumulates in vulnerable neurons in Alzheimer's disease. *Alzheimers Dement.* **16**, 273–282 (2020).
68. I. Lauritzen *et al.*, Intraneuronal aggregation of the β-CTF fragment of APP (C99) induces Aβ-independent lysosomal-autophagic pathology. *Acta Neuropathol.* **132**, 257–276 (2016).
69. L. Vaillant-Beuchot *et al.*, Accumulation of amyloid precursor protein C-terminal fragments triggers mitochondrial structure, function, and mitophagy defects in Alzheimer's disease models and human brains. *Acta Neuropathol.* **141**, 39–65 (2021).
70. P. Melnyk *et al.*, Chloroquine and chloroquinoline derivatives as models for the design of modulators of amyloid Peptide precursor metabolism. *ACS Chem. Neurosci.* **6**, 559–569 (2015).
71. C. Evrard *et al.*, Contribution of the endosomal-lysosomal and proteasomal systems in amyloid-β precursor protein derived fragments processing. *Front. Cell. Neurosci.* **12**, 435 (2018).
72. F. Gebauer, T. Schwarzl, J. Valcárcel, M. W. Hentze, RNA-binding proteins in human genetic disease. *Nat. Rev. Genet.* **22**, 185–198 (2021).
73. D. Cook *et al.*, FXR1P limits long-term memory, long-lasting synaptic potentiation, and de novo GluA2 translation. *Cell Rep.* **9**, 1402–1416 (2014).
74. J. Sopova *et al.*, RNA-binding protein FXR1 is presented in rat brain in amyloid form. *Sci. Rep.* **9**, 18983 (2019).
75. J. Y. Kang *et al.*, LLPS of FXR1 drives spermiogenesis by activating translation of stored mRNAs. *Science* **377**, eabj6647 (2022).
76. K. Leppek, R. Das, M. Barna, Functional 5′ UTR mRNA structures in eukaryotic translation regulation and how to find them. *Nat. Rev. Mol. Cell Biol.* **19**, 158–174 (2018).
77. I. N. Shatsky, I. M. Terenin, V. V. Smirnova, D. E. Andreev, Cap-independent translation: What's in a name? *Trends Biochem. Sci.* **43**, 882–895 (2018).